

## Compensation in Al-Doped ZnO by Al-Related Acceptor Complexes: Synchrotron X-Ray Absorption Spectroscopy and Theory

J. T-Thienprasert,<sup>1,2</sup> S. Rujirawat,<sup>3</sup> W. Klysubun,<sup>4</sup> J. N. Duenow,<sup>5</sup> T. J. Coutts,<sup>5</sup> S. B. Zhang,<sup>6</sup>  
D. C. Look,<sup>7</sup> and S. Limpijumnong<sup>3</sup>

<sup>1</sup>*Department of Physics, Kasetsart University, Bangkok 10900, Thailand*

<sup>2</sup>*Thailand Center of Excellence in Physics (ThEP Center), Commission on Higher Education, Bangkok 10400, Thailand*

<sup>3</sup>*School of Physics, Suranaree University of Technology, Nakhon Ratchasima 30000, Thailand*

<sup>4</sup>*Synchrotron Light Research Institute, Nakhon Ratchasima 30000, Thailand*

<sup>5</sup>*National Renewable Energy Laboratory, Golden, Colorado 80401, USA*

<sup>6</sup>*Physics Department, Rensselaer Polytechnic Institute, Troy, New York 12180, USA*

<sup>7</sup>*Semiconductor Research Center, Wright State University, Dayton, Ohio 45435, USA*

(Received 29 August 2012; published 28 January 2013)

The synchrotron x-ray absorption near edge structures (XANES) technique was used in conjunction with first-principles calculations to characterize Al-doped ZnO films. Standard characterizations revealed that the amount of carrier concentration and mobility depend on the growth conditions, i.e. H<sub>2</sub> (or O<sub>2</sub>)/Ar gas ratio and Al concentration. First-principles calculations showed that Al energetically prefers to substitute on the Zn site, forming a donor Al<sub>Zn</sub>, over being an interstitial (Al<sub>i</sub>). The measured Al *K*-edge XANES spectra are in good agreement with the simulated spectra of Al<sub>Zn</sub>, indicating that the majority of Al atoms are substituting for Zn. The reduction in carrier concentration or mobility in some samples can be attributed to the Al<sub>Zn</sub>-V<sub>Zn</sub> and 2Al<sub>Zn</sub>-V<sub>Zn</sub> complex formations that have similar XANES features. In addition, XANES of some samples showed additional features that are the indication of some α-Al<sub>2</sub>O<sub>3</sub> or *n*Al<sub>Zn</sub>-O<sub>i</sub> formation, explaining their poorer conductivity.

DOI: [10.1103/PhysRevLett.110.055502](https://doi.org/10.1103/PhysRevLett.110.055502)

PACS numbers: 61.72.-y, 61.05.cj

Transparent conductive oxides (TCOs) are needed in many applications, for instance, touch screens, solar cells, and photovoltaic devices [1–3]. The most commonly used TCO is indium tin oxide. Recently, ZnO was extensively studied for its TCO aspects, in hope of replacing indium tin oxide, because it is nontoxic, low cost, and abundant. As-grown ZnO is an *n*-type wide band gap (~ 3.3 eV) semiconductor where its conductivity is believed to originate mainly from the intrinsic defects or unintentional hydrogen impurity [4–6]. Native defects and unintentional impurities in ZnO have also been studied theoretically [6–9]. A highly conductive ZnO thin film with high transmittance in the visible light region can be achieved by doping with group-III elements. Among group-III doped ZnO, Al-doped ZnO (AZO) emerged as the most promising candidate due to its high temperature stability and the fact that Al is abundant. There are several deposition techniques that have been reported to successfully produce AZO thin films. These include chemical vapor deposition [10], magnetron sputtering [11], spray pyrolysis [12], and pulsed laser deposition [13].

Partial information on how during-growth and post-growth conditions (such as oxygen partial pressure and ultraviolet-ozone treatment) affect AZO film quality is reported [1,13]. However, none of the previous studies offers the detailed information on the local structure of Al site in ZnO crystal. In this Letter, a combination of Al *K*-edge x-ray absorption near edge structures (XANES)

and first-principles calculations was used to investigate the rf-magnetron sputtered AZO films grown under different conditions (H<sub>2</sub>/Ar or O<sub>2</sub>/Ar gas) and with different Al concentrations. This work illustrates that the combined systematic XANES measurements and first-principles calculations can be used to identify the local structures of impurities that should have broad applications for many systems.

AZO films were grown by rf-magnetron sputtering using an oxide target with Argon as the primary sputtering gas. To manipulate the growth condition (O rich or O poor), small amounts of O<sub>2</sub> or H<sub>2</sub> were added to the Ar at different ratios. All films were deposited on Corning glass (7059 or 1737) with the substrate temperature of 200 °C. The carrier concentration and mobility of the films were measured with the detail described in Ref. [14].

To study the effects of Al content, we examined four films grown with varied Al content from 0.1 to 2.0 wt%. The weight percents were calculated from the weight of Al<sub>2</sub>O<sub>3</sub> versus ZnO in the starting material. The sputtering gas was fixed at the H<sub>2</sub>/Ar gas ratio of 0.3%. The concentration and mobility are shown in Table I and Fig. 1. The Al content is labeled at the end of the sample name. As the Al content increased by 20 times, i.e. from 0.1% to 2.0%, the carrier concentration increased but by only 7 times, i.e. from  $1.1 \times 10^{20} \text{ cm}^{-3}$  to  $7.3 \times 10^{20} \text{ cm}^{-3}$ , accompanied by the reduction in electron mobility by about half, i.e. from 52 to 25 cm<sup>2</sup> V<sup>-1</sup> s<sup>-1</sup>.

TABLE I. The growth condition for Al-doped ZnO thin films. The carrier concentration and mobility of each sample depend on the growth conditions.

Sample name	Al <sub>2</sub> O <sub>3</sub> content (wt %)	Sputtering gas	Film thickness (nm)	Carrier concentration (cm <sup>-3</sup> )	Mobility (cm <sup>2</sup> V <sup>-1</sup> s <sup>-1</sup> )
OP-a/2.0	2.0	0.3% H <sub>2</sub> /Ar	430	$7.3 \times 10^{20}$	25
OP-a/1.0	1.0	0.3% H <sub>2</sub> /Ar	490	$5.5 \times 10^{20}$	32
OP-a/0.5	0.5	0.3% H <sub>2</sub> /Ar	410	$3.4 \times 10^{20}$	36
OP-a/0.1	0.1	0.3% H <sub>2</sub> /Ar	370	$1.1 \times 10^{20}$	52
OP-b/1.0	1.0	1% H <sub>2</sub> /Ar	430	$5.7 \times 10^{20}$	20
OP-a/1.0	1.0	0.3% H <sub>2</sub> /Ar	490	$5.5 \times 10^{20}$	32
OFix/1.0	1.0	100% Ar	610	$4.4 \times 10^{20}$	29
OR-a/1.0	1.0	0.3% O <sub>2</sub> /Ar	520	$2.3 \times 10^{19}$	0.1
OR-b/1.0	1.0	0.5% O <sub>2</sub> /Ar	480	$7.3 \times 10^{18}$	0.1

To study the effects of growth conditions, we fixed the Al content at 1.0 wt% and examined five samples that were grown with varied sputtering gas ratios, starting from O<sub>2</sub> rich (O<sub>2</sub>/Ar = 0.5%) to pure Ar to O<sub>2</sub> poor (H<sub>2</sub>/Ar = 1%); H<sub>2</sub> is used to suppress O<sub>2</sub> released from the sputtering target. The sample names are labeled to reflect these sputtering gas ratios, i.e., OP = O poor, OR = O rich, and OFix = pure Ar. It was found that the carrier concentration increased by nearly 2 orders of magnitude, i.e. from  $7.3 \times 10^{18}$  cm<sup>-3</sup> to  $5.7 \times 10^{20}$  cm<sup>-3</sup> as the sputtering gas changed from O<sub>2</sub>-rich to O-poor conditions. The mobility was near zero under the O-rich conditions and rapidly increased under pure Ar and H<sub>2</sub>/Ar conditions with the highest value taking place when the sputtering gas contained a 0.3% H<sub>2</sub>/Ar ratio (labeled OP-a).

All of the films were characterized by x-ray absorption measurements in the fluorescent mode with a 13-component Ge detector (Canberra) at beam line #8 of the Siam Photon Source (electron energy of 1.2 GeV, beam

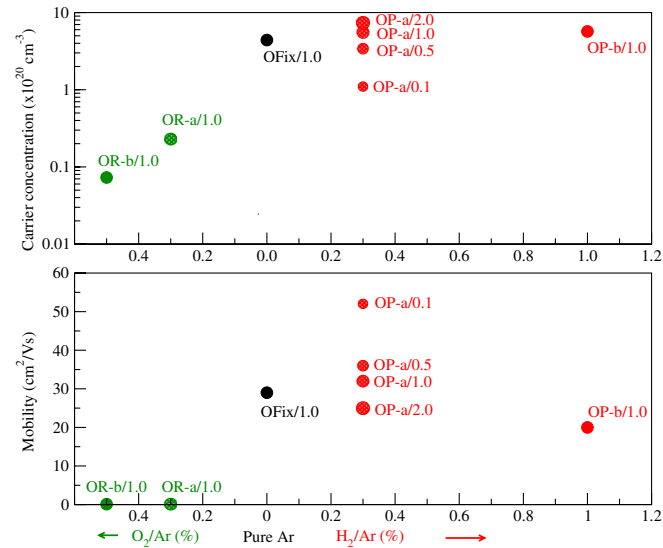


FIG. 1 (color online). The carrier concentration (top) and mobility (bottom) of samples grown with different sputtering gas and Al concentrations.

current 80–120 mA) of the Synchrotron Light Research Institute, Thailand [15]. A double crystal monochromator KTiOPO<sub>4</sub> was used to scan the synchrotron x ray with the photon energy step of 0.25 eV in the range of 1550–1610 eV, covering the XANES region of Al *K*-edge. The measured spectra are shown in Figs. 2(a) and 2(b). In general, all measured spectra composed of two peaks, labeled P1 and P2.

In order to relate the observed spectra to the local structure around the Al atom, we performed first-principles calculations [16]. Two computational codes, i.e. the Vienna *ab initio* simulation package (VASP) [17,18] and the FEFF8.2 codes [19,20], were employed in series. The VASP codes were used to optimize the detailed relaxation of the defect structures as well as to determine their energetic stability. The FEFF8.2 codes were used to simulate the XANES spectra from the relaxed local structures obtained from VASP. In VASP calculations, the density functional theory (DFT) within the local density approximation (LDA) for the exchange-correlation functional was used. The atomic potentials used in these calculations were the ultrasoft

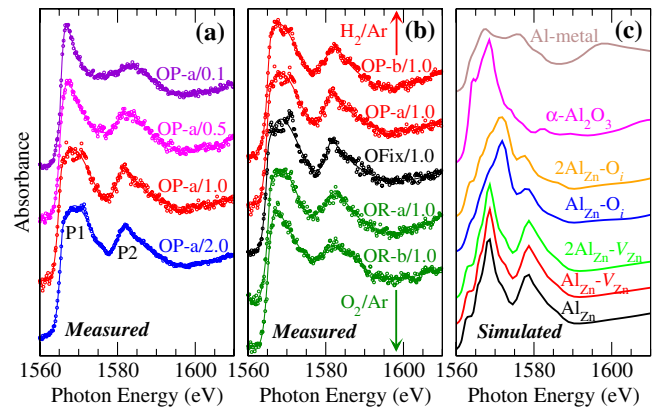


FIG. 2 (color online). (a) The measured Al *K*-edge XANES spectra of samples grown under 0.3% H<sub>2</sub>/Ar sputtering gas with varied Al contents from 0.1% to 2.0%. (b) The spectra of samples with Al content of 1.0% grown under different sputtering gas conditions from O poor to O rich. (c) The simulated spectra from different local structure models of Al.

pseudopotential with projector-augmented wave [21], allowing a rather low energy cutoff of 500 eV for the plane-wave basis set. The calculated lattice parameters of bulk ZnO are  $a = 3.21$  and  $c/a = 1.61$  Å, which are in good agreement with the experimental values of  $a = 3.25$  and  $c/a = 1.60$  Å [22]. To study defects, we used the supercell approach with a 96-atom supercell. The Monkhorst-Pack scheme [23] with a shifted sampling mesh of  $2 \times 2 \times 2$  was used for  $k$ -space integrations. All atoms in the supercell were allowed to relax until the Hellmann-Feynman [24] forces became less than  $10^{-3}$  eV/Å. After the optimized structures were obtained, the coordinates were ported into the FEFF8.2 code for XANES spectra simulation. The FEFF8.2 code is based on the multiple-scattering expansion with the muffin-tin potentials. The Hedin-Lundqvist was used as the exchange potential with an imaginary part of 0.5 eV to simulate the experimental broadening. The radii of self-consistent muffin-tin atomic potential and full-multiple scattering were set at 0.55 and 0.80 nm, respectively.

The obvious choices for the possible forms of Al in ZnO are Al substitution for Zn ( $\text{Al}_{\text{Zn}}$ ), phase separated  $\alpha\text{-Al}_2\text{O}_3$ , and metal Al. These crystal structures were first calculated and optimized using the VASP codes. After that, the corresponding XANES spectra [Fig. 2(c)] were simulated using the FEFF8.2 codes. The simulated spectrum of  $\text{Al}_{\text{Zn}}$  contains two peaks that are consistent with  $P1$  and  $P2$  observed in the Al-doped ZnO samples. On the other hand, the simulated spectrum of  $\alpha\text{-Al}_2\text{O}_3$  contains only one large broad peak at the energy near the  $P1$  peak and that of metal Al has broad features without any sharp peak. Among three spectra, it is clear that only the simulated XANES spectrum of  $\text{Al}_{\text{Zn}}$  has an overall feature consistent with the measured XANES spectra. To understand the source of the differences between the two-peak ( $P1$  and  $P2$ ) feature in the  $\text{Al}_{\text{Zn}}$  spectrum and the single broad peak feature in the  $\alpha\text{-Al}_2\text{O}_3$  spectrum, we investigated the electronic states associated with them. The site-projected partial density of unoccupied  $p$ -states (PDOS) plots around the Al atom, based on VASP calculations (following Ref. [25] that describes the case of Mn in  $\text{PbTiO}_3$ ) of  $\text{Al}_{\text{Zn}}$  in ZnO and  $\alpha\text{-Al}_2\text{O}_3$  are shown in Figs. 3(a) and 3(b), respectively. For  $\text{Al}_{\text{Zn}}$ , the unoccupied  $p$  states around the fourfold Al atom can be split into two groups, the lower energy ( $P1$ ) and the higher energy ( $P2$ ) ones. The charge density plot shows that the lower energy group of states is localized in the region away from the Al-O bonds while the higher energy group of states is localized closer to the bonds. On the other hand, for the sixfold Al in  $\text{Al}_2\text{O}_3$ , the unoccupied  $p$  states are more symmetric and are localized away from the bonds without the group of higher energy ones.

Figure 2(a) shows the measured spectra of the samples with varied Al content from 0.1% to 2.0%. The  $P1$  peak is the sharpest for the 0.1% sample and becomes broader in samples with higher Al content. The broadening of the  $P1$

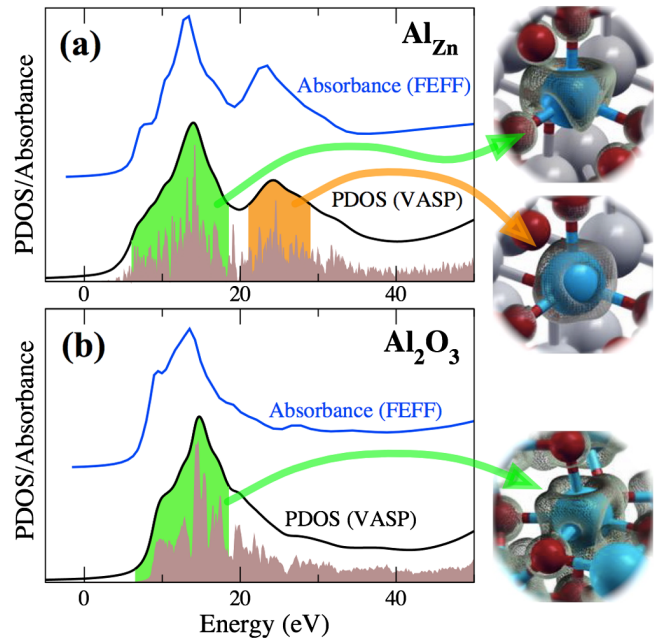


FIG. 3 (color online). Calculated Al site and angular momentum ( $l = 1$ ) projected partial density of states (PDOS) based on VASP and simulated absorption spectra based on FEFF of (a)  $\text{Al}_{\text{Zn}}$  in ZnO and (b) Al in  $\alpha\text{-Al}_2\text{O}_3$ . PDOSs are broadened (originals shown under each curve) and shown relative to the valence band maximum; the absorbances are shifted for ease of comparison. The electron density associated with the peaks  $P1$  and  $P2$  for  $\text{Al}_{\text{Zn}}$  and  $P1$  for  $\text{Al}_2\text{O}_3$  are shown in the insets.

peak as Al content increases is an indication of the second form of Al in addition to  $\text{Al}_{\text{Zn}}$ . The most probable candidates are  $\text{Al}_2\text{O}_3$  and  $n\text{Al}_{\text{Zn}}\text{-O}_i$  ( $n = 1$  or  $2$ ) complexes in ZnO where their main features contain a broader peak centering near  $P1$  as shown in Fig. 2(c). The formation of the phase-separated  $\text{Al}_2\text{O}_3$  or  $n\text{Al}_{\text{Zn}}\text{-O}_i$  (poorer crystal quality) is consistent with the observed lower carrier mobility as the Al content increases. The formation of unwanted  $\text{Al}_2\text{O}_3$  or  $n\text{Al}_{\text{Zn}}\text{-O}_i$ , which competes the formation of the desired  $\text{Al}_{\text{Zn}}$ , explains why the carrier concentration increases by only 7 times as the Al concentration increases by 20 times.

Figure 2(b) shows the measured spectra of the samples grown with 1.0% Al content but with different sputtered gas conditions, from O rich to O poor. The  $P1$  peaks of all samples are broad (slightly sharper for the samples grown under O-rich conditions), suggesting that the samples contain  $\text{Al}_{\text{Zn}}$  with a small amount of  $\text{Al}_2\text{O}_3$  (or  $n\text{Al}_{\text{Zn}}\text{-O}_i$ ). The spectra from samples with different sputtered gas conditions are quite similar, suggesting similar fraction-of-phase-separated  $\text{Al}_2\text{O}_3$  (or  $n\text{Al}_{\text{Zn}}\text{-O}_i$ ). However, the carrier concentration and mobility are greatly varied with the sputtered gas conditions. The variation of the carrier concentration and mobility indicates the formation of defect complexes between  $\text{Al}_{\text{Zn}}$  and native defect(s) or the passivation of  $\text{Al}_{\text{Zn}}$  by native defect(s). For example, a deep

double acceptor Zn vacancy ( $V_{\text{Zn}}$ ) can bind with  $\text{Al}_{\text{Zn}}$  forming either  $\text{Al}_{\text{Zn}}-V_{\text{Zn}}$  (single acceptor) or  $2\text{Al}_{\text{Zn}}-V_{\text{Zn}}$  (neutral) defect complexes.

To evaluate the formation nature of defects and defect complexes under different growth conditions, we calculated the formation energy of each defect defined [26] as

$$\Delta H_f = E_{\text{tot}}(D^q) - E_{\text{tot}}(0) - \sum \Delta n_x \mu_x + q(E_f + E_v), \quad (1)$$

where  $E_{\text{tot}}(D^q)$  is the calculated total energy of a supercell containing a defect  $D$  in charge state  $q$ ,  $E_{\text{tot}}(0)$  is the calculated total energy of the same supercell without a defect, and  $\Delta n_x$  is the number of atoms from species  $X$  ( $= \text{Zn}, \text{O},$  or  $\text{Al}$ ) being added to (negative sign = removed from) a supercell to form the defect cell.  $\mu_x$  is the reservoir chemical potential of specie  $X$ ,  $E_f$  is the electron Fermi energy, and  $E_v$  is the valence band maximum (VBM) of ZnO (here, we adopted the approach used in Ref. [26] for the VBM determination as well as the energy alignment between the defect supercell and defect-free supercell). Although DFT-LDA calculations strongly underestimated a bulk ZnO band gap ( $E_{g,\text{LDA}} = 0.9$  eV), test calculations using a hybrid-functional approach shows that our calculated formation energies remain accurate to within 0.2 eV, and the main conclusion drawn in this work is not affected by the band gap underestimation [27].

The upper limits for  $\mu_{\text{Zn}}$ ,  $\mu_{\text{O}}$ , and  $\mu_{\text{Al}}$  are the energies of solid Zn, gaseous  $\text{O}_2$ , and solid Al, which we referenced as the zero point. To grow ZnO in equilibrium, it is required that  $\mu_{\text{Zn}} + \mu_{\text{O}} = \mu_{\text{ZnO}}$ , where the calculated ZnO heat of formation is  $\mu_{\text{ZnO}} = -3.53$  eV. Therefore, in our calculations, we have  $\mu_{\text{Zn}} = -3.53$  eV  $- \mu_{\text{O}}$ , where  $-3.53$  eV  $\leq \mu_{\text{O}} \leq 0$  (note that  $\mu_{\text{O}} = 0$  is defined as half of the  $\text{O}_2$  energy). In the presence of O, Al prefers to form  $\text{Al}_2\text{O}_3$  over solid Al. Therefore, the upper limit of  $\mu_{\text{Al}}$  is set by  $\text{Al}_2\text{O}_3$  precipitation limits, i.e.  $\mu_{\text{Al}}^{\text{max}} = [\mu_{\text{Al}_2\text{O}_3} - 3\mu_{\text{O}}]/2$ . For zinc-rich conditions ( $\mu_{\text{Zn}} = 0$ ),  $\mu_{\text{Al}}^{\text{max}} = -3.44$  eV. For oxygen-rich conditions ( $\mu_{\text{O}} = 0$ ),  $\mu_{\text{Al}}^{\text{max}} = -8.73$  eV.

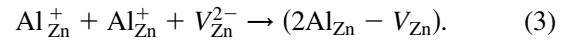
The calculated total energies are shown in detail in the Supplemental Material [27]. The calculations show that  $\text{Al}_{\text{Zn}}$  is a single shallow donor without the transition energy in the gap. Zn vacancy ( $V_{\text{Zn}}$ ) is an acceptor with two transition energies at  $\varepsilon(0/1^-) = 0.09$  eV and  $\varepsilon(1^-/2^-) = 0.38$  eV. O interstitial ( $\text{O}_i$ ) is a deeper acceptor with two transition energies at  $\varepsilon(0/1^-) = 0.27$  eV and  $\varepsilon(1^-/2^-) = 0.87$  eV.

Under Zn-rich conditions, the formation energy of  $\text{Al}_{\text{Zn}}$  is the lowest one for semi-insulating to  $n$ -type samples, i.e., when the Fermi energy is in the range from around mid gap to the conduction band minimum. The formation energy of the interstitial Al ( $\text{Al}_i$ ) is several eV higher than  $\text{Al}_{\text{Zn}}$  under this condition (see Ref. [27]). Therefore, the  $\text{Al}_{\text{Zn}}$  donor is expected to be the dominant defect form. Because the formation energies of  $V_{\text{Zn}}$  and  $\text{O}_i$  that are native acceptors

are high in this growth condition, they would not form in a significant amount and the sample would remain in a good  $n$ -type condition. Interestingly,  $\text{Al}_{\text{Zn}}$  formation energy is lower under Zn-rich conditions than under O-rich conditions. This is quite counterintuitive because generally one would expect the Al to have the best chance to substitute for a Zn site when there is less Zn to compete with, i.e., Zn-poor conditions. However, for this particular case, the chemical potential of Al is limited by the O chemical potential due to the  $\text{Al}_2\text{O}_3$  precipitation limit. The highest possible  $\mu_{\text{Al}}$  requires the lowest  $\mu_{\text{O}}$ , i.e. Zn-rich conditions.

Under O-rich conditions, the formation energy of  $\text{Al}_{\text{Zn}}$  is higher than the native acceptors  $V_{\text{Zn}}$  and  $\text{O}_i$  under  $n$ -type conditions (high Fermi energy). As a result,  $V_{\text{Zn}}$  and  $\text{O}_i$  could form and either compensate or passivate  $\text{Al}_{\text{Zn}}$  leading to lower  $n$ -type conductivity. Because  $V_{\text{Zn}}$  has lower formation energy, it is more likely to form than  $\text{O}_i$ .

When coexisted,  $\text{Al}_{\text{Zn}}$  and  $V_{\text{Zn}}$  can form defect complexes via the following reactions:



Equations (2) and (3) are exothermic with binding energies 0.53 and 1.19 eV, respectively, assuming the Fermi energy is at the conduction band minimum. These binding energies give the maximum passivation efficiency  $\kappa_D^{\text{max}}$ , defined in Ref. [28], of about 0.9 (calculated using the growth temperature of 200 °C), suggesting that the complex could potentially form. The  $\text{Al}_{\text{Zn}}-V_{\text{Zn}}$  complex is a deep acceptor with the transition energy at  $\varepsilon(0/1^-) = 0.39$  eV. On the other hand, the  $2\text{Al}_{\text{Zn}}-V_{\text{Zn}}$  complex is neutral. In a similarly manner,  $\text{Al}_{\text{Zn}}$  and  $\text{O}_i$  can form an electrically amphoteric  $\text{Al}_{\text{Zn}}-\text{O}_i$  complex with the transition energy at  $\varepsilon(1^-/1^-) = 0.72$  eV.  $\text{Al}_{\text{Zn}}-\text{O}_i$  can further bind another  $\text{Al}_{\text{Zn}}$  and form a  $2\text{Al}_{\text{Zn}}-\text{O}_i$  complex, which is neutral. The binding energy of  $\text{Al}_{\text{Zn}}-\text{O}_i$  and  $2\text{Al}_{\text{Zn}}-\text{O}_i$  are as large as 1 and 2 eV, respectively (depending on the Fermi energy (see Ref. [27])). The formation of these  $\text{Al}_{\text{Zn}}-V_{\text{Zn}}$  and  $\text{Al}_{\text{Zn}}-\text{O}_i$  complex defects would suppress the  $n$ -type carriers leading to poorer  $n$ -type conductivity.

Because the above mentioned complexes, i.e.  $\text{Al}_{\text{Zn}}-V_{\text{Zn}}$ ,  $2\text{Al}_{\text{Zn}}-V_{\text{Zn}}$ ,  $\text{Al}_{\text{Zn}}-\text{O}_i$ , and  $2\text{Al}_{\text{Zn}}-\text{O}_i$ , are bound and can potentially be formed, we simulated their XANES spectra [also shown in Fig. 2(c)]. The XANES spectra of  $\text{Al}_{\text{Zn}}-V_{\text{Zn}}$  and  $2\text{Al}_{\text{Zn}}-V_{\text{Zn}}$  complexes are very similar to that of  $\text{Al}_{\text{Zn}}$  since the vacancies are the second neighbors to the  $\text{Al}_{\text{Zn}}$  and the local structure of the Al atom remains fourfolded. On the other hand, the XANES spectra of  $\text{Al}_{\text{Zn}}-\text{O}_i$  and  $2\text{Al}_{\text{Zn}}-\text{O}_i$  complexes are quite distinct from that of  $\text{Al}_{\text{Zn}}$ . The O interstitial is situated next to  $\text{Al}_{\text{Zn}}$ , increasing the coordination of the Al atom to 5. The increase in coordination number limits the split of the unoccupied  $p$  states around the Al atom in a similar way as the sixfold Al in  $\alpha\text{-Al}_2\text{O}_3$ . As a result, the XANES spectra of  $\text{Al}_{\text{Zn}}-\text{O}_i$  and

$2\text{Al}_{\text{Zn}}\text{-O}_i$  complexes contain one large broad low-energy peak similar to the spectrum of  $\alpha\text{-Al}_2\text{O}_3$  and a much reduced  $P2$  peak.

The formation energy calculations and XANES simulations show the following. (1) Zn-rich condition is the most favorable condition for  $\text{Al}_{\text{Zn}}$  to form. (2) Under O-rich conditions, native acceptor defects  $V_{\text{Zn}}$  and  $\text{O}_i$  have low energy and can either compensate or passivate  $\text{Al}_{\text{Zn}}$  (forming  $n\text{Al}_{\text{Zn}}\text{-}V_{\text{Zn}}$  or  $n\text{Al}_{\text{Zn}}\text{-O}_i$  complexes) reducing the conductivity and mobility of the sample. (3) The simulated XANES spectra of  $n\text{Al}_{\text{Zn}}\text{-}V_{\text{Zn}}$  is almost identical to that of  $\text{Al}_{\text{Zn}}$ . This explains why samples grown under O-rich conditions can have similar XANES spectra to those grown under O-poor conditions despite its much lower values of mobility and conductivity. (4) The simulated XANES spectra of  $n\text{Al}_{\text{Zn}}\text{-O}_i$ , which has fivefolded Al, is similar to that of  $\alpha\text{-Al}_2\text{O}_3$  (sixfold). This shows that the broadening of the first peak in some samples is the indicator of the higher coordinated Al that can be either phase-separated  $\alpha\text{-Al}_2\text{O}_3$  or defect complexes such as  $n\text{Al}_{\text{Zn}}\text{-O}_i$ , both of which lead to lower conductivity and mobility.

In summary, Al-doped ZnO thin films prepared by rf-magnetron sputtering under different growth conditions and Al contents were studied by Al  $K$ -edge x-ray absorption spectroscopy in the near edge region. First-principles total energy calculations and XANES simulations were employed to relate the measured results to the local atomic structures. The formation energy of  $\text{Al}_{\text{Zn}}$  is the lowest under Zn-rich conditions in agreement with the experimental observation that a better  $n$ -type Al-doped ZnO film is grown under Zn-rich conditions. The measured XANES spectra consist of two peaks in agreement with the simulation of a  $\text{Al}_{\text{Zn}}$  spectrum. In films with higher Al contents, the low energy peak is broadening, which could be the indication of some phase-separated  $\alpha\text{-Al}_2\text{O}_3$  or  $n\text{Al}_{\text{Zn}}\text{-O}_i$  complex formation. For films grown under O-rich conditions, the poorer  $n$ -type conductivity could be attributed to the formation of  $n\text{Al}_{\text{Zn}}\text{-}V_{\text{Zn}}$  complexes that are not donors and have an almost identical XANES spectrum to that of  $\text{Al}_{\text{Zn}}$ .

One of the authors (S.B.Z.) is supported by the Department of Energy under Grant No. DE-SC0002623.

---

[1] G. B. Murdoch, S. Hinds, E. H. Sargent, S. W. Tsang, L. Mordoukhovski, and Z. H. Lu, *Appl. Phys. Lett.* **94**, 213301 (2009).

[2] G. K. R. Senadeera, K. Nakamura, T. Kitamura, Y. Wada, and S. Yanagida, *Appl. Phys. Lett.* **83**, 5470 (2003).

[3] K. Tonooka, H. Bando, and Y. Aiura, *Thin Solid Films* **445**, 327 (2003).

[4] D. C. Reynolds, D. C. Look, B. Jogai, and H. Morkoç, *Solid State Commun.* **101**, 643 (1997).

[5] D. C. Look, *Mater. Sci. Eng. B* **80**, 383 (2001).

[6] A. Janotti and C. G. Van de Walle, *Phys. Rev. B* **76**, 165202 (2007).

[7] A. F. Kohan, G. Ceder, D. Morgan, and Chris G. Van deWalle, *Phys. Rev. B* **61**, 15019 (2000).

[8] C. G. Van de Walle, *Phys. Rev. Lett.* **85**, 1012 (2000).

[9] S. Limpijumnong and S. B. Zhang, *Appl. Phys. Lett.* **86**, 151910 (2005).

[10] J. Hu and R. G. Gordon, *J. Appl. Phys.* **71**, 880 (1992).

[11] Y. Igasaki and H. Saito, *J. Appl. Phys.* **70**, 3613 (1991).

[12] A. F. Aktaruzzaman, G. L. Sharma, and L. K. Malhotra, *Thin Solid Films* **198**, 67 (1991).

[13] A. V. Singh, R. M. Mehra, N. Buthrath, A. Wakahara, and A. Yoshida, *J. Appl. Phys.* **90**, 5661 (2001).

[14] J. N. Duenow, T. A. Gessert, D. M. Wood, A. C. Dillon, and T. J. Coutts, *J. Vac. Sci. Technol. A* **26**, 692 (2008).

[15] W. Klysubun, P. Tarawarakarn, P. Sombunchoo, S. Klinkhieo, J. Chairapa, and P. Songsiriritthigul, *AIP Conf. Proc.* **879**, 860 (2007).

[16] C. G. Van de Walle and J. Neugebauer, *J. Appl. Phys.* **95**, 3851 (2004).

[17] G. Kresse and J. Furthmüller, *Comput. Mater. Sci.* **6**, 15 (1996).

[18] G. Kresse and J. Hafner, *J. Phys. Condens. Matter* **6**, 8245 (1994).

[19] A. L. Ankudinov, C. E. Bouldin, J. J. Rehr, J. Sims, and H. Hung, *Phys. Rev. B* **65**, 104107 (2002).

[20] A. L. Ankudinov, B. Ravel, J. J. Rehr, and S. D. Conradson, *Phys. Rev. B* **58**, 7565 (1998).

[21] G. Kresse and D. Joubert, *Phys. Rev. B* **59**, 1758 (1999).

[22] O. Madelung, M. Schulz, and H. Weiss, *Numerical Data and Functional Relationships in Science and Technology* (Springer-Verlag, Berlin, 1982), Vol. 17.

[23] H. J. Monkhorst and J. D. Pack, *Phys. Rev. B* **13**, 5188 (1976).

[24] R. P. Feynman, *Phys. Rev.* **56**, 340 (1939).

[25] S. Limpijumnong, S. Rujirawat, A. Boonchun, M. F. Smith, and B. Cherdhirunkorn, *Appl. Phys. Lett.* **90**, 103113 (2007).

[26] S. B. Zhang, *J. Phys. Condens. Matter* **14**, R881 (2002).

[27] See Supplemental Material at <http://link.aps.org/supplemental/10.1103/PhysRevLett.110.055502> for the calculated defect formation energy.

[28] T.-L. Chan, D. West, and S. B. Zhang, *Phys. Rev. Lett.* **107**, 035503 (2011).